Solar RRL
www.solar-rrl.com

The Microstructure of Underdense Hydrogenated Amorphous Silicon and its Application to Silicon Heterojunction Solar Cells

Benedikt Fischer, Wolfhard Beyer, Andreas Lambertz, Maurice Nuys, Weiyuan Duan, Kaining Ding, and Uwe Rau*

Dedicated to Dr. Wolfhard Beyer, who passed away in the course of the publication process

The application of thin underdense hydrogenated amorphous silicon (a-Si:H) films for passivation of crystalline Si (c-Si) by avoiding epitaxy in silicon heterojunction (SHJ) solar cell technology has recently been proposed and successfully applied. Herein, the microstructure of such underdense a-Si:H films, as used in our silicon heterojunction solar cell baseline, is investigated mainly by Raman spectroscopy, effusion, and secondary ion mass spectrometry. In H effusion experiments, a low-temperature (near 400 °C) effusion peak which has been attributed to the diffusion of molecular H_2 through a void network is seen. The dependence of the H effusion peaks on film thickness is similar as observed previously for void rich, low substrate-temperature a-Si:H material. Solar cells using underdense a-Si:H as i1-layer with a maximum efficiency of 24.1% are produced. The passivation quality of the solar cells saturates with increasing i1-layer thickness. The fact that with such underdense material combined with a following high-quality i2-layer, instead of only high-quality a-Si:H with a low defect density direct on the c-Si substrate, good passivation of c-Si solar cells is achieved, which demonstrates that in the passivation process, molecular hydrogen plays an important role.

1. Introduction

The use of porous a-Si:H films with high hydrogen content to prevent epitaxy has been proposed several times.[1–3] Recently, such material was termed "underdense" by Liu et al.[1] in connection with optical density measurements using the method of Remeš et al.[4] "Underdense" means that the material has many large voids and low mass density in contrast to standard a-Si:H with a mass density of $\approx 2.29\,\mathrm{g\,cm^{-3}}$.[1,5,6] The mass densities of the a-Si:H films in this work are $2.1–2.2\,\mathrm{g\,cm^{-3}}$ and can therefore all be termed "underdense." However, a reduction in density of (plasma grown) a-Si:H films for reduced substrate temperatures and/or enhanced hydrogen content is long known.[7] It was found that in such material hydrogen diffusion is not by motion of H atoms but of H_2 molecules.[8] To clarify the microstructure of "underdense" a-Si:H, as used in SHJ solar cells,[1–3] we applied Raman spectroscopy, hydrogen effusion, and other methods. We investigate layers of underdense a-Si:H with thicknesses from 2.3 to 150 nm grown at different plasma powers and on various substrates. We use effusion measurements in particular to compare the properties of the present a-Si:H with previously investigated a-Si:H material. Additionally, we used underdense a-Si:H for the i1-layer on the *p*-side of SHJ solar cells as shown in **Figure 1** with a maximum efficiency of 24.1% on an area of $(15.7 \times 15.7)\,\mathrm{cm^2}$. The i1-layer on the n-side was kept constant to ensure a clear comparison of the different i1-layers on the p-side.

2. Results

The growth of amorphous silicon layers can depend on the underlying substrate due to differences in nucleation.[9,10] To investigate the growth process of underdense a-Si:H, we deposited films ($d = 5–8$ nm) using different plasma powers on HF-etched c-Si (with HF), c-Si with native oxide (w/o HF), and glass. **Figure 2** shows the corresponding Raman spectra

B. Fischer, W. Beyer†, A. Lambertz, M. Nuys, W. Duan, K. Ding, U. Rau
Institut für Energie- und Klimaforschung (IEK-5)
Forschungszentrum Jülich
52428 Jülich, Germany
E-mail: b.fischer@fz-juelich.de

U. Rau
Faculty of Electrical Engineering and Information Technology
RWTH Aachen University
52074 Aachen, Germany

The ORCID identification number(s) for the author(s) of this article can be found under https://doi.org/10.1002/solr.202300103.

†Deceased December 9, 2022.

DOI: 10.1002/solr.202300103

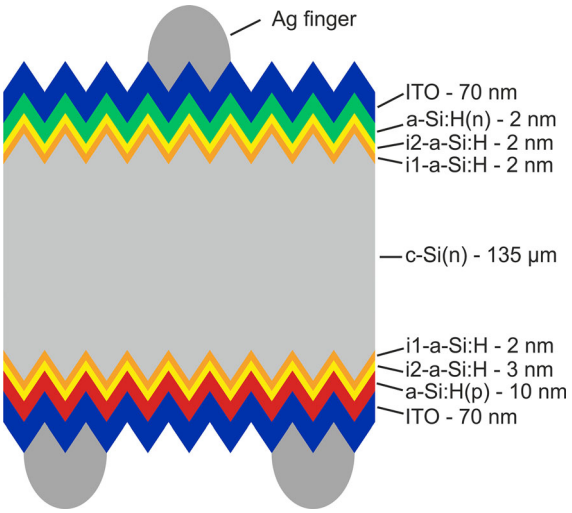

Figure 1. Schematic of a SHJ solar cell and its layer stack.

for wavelengths from 1900 to 2200 cm^{-1}. Three different plasma powers (200, 300, and 400 W) were applied, which were expected to result in different microstructures. Indeed, for the 200 W layer, the 2100 cm^{-1} peak is dominant, the 300 W layer shows a balanced ratio for the 2000 and 2100 cm^{-1} peak intensity, and for the 400 W layer the 2000 cm^{-1} peak is dominant. However, on all substrate materials, the spectra are similar, indicating a growth independent of the substrate material.

The microstructure parameter measured by Raman spectroscopy decreases with increasing plasma power, as shown in **Figure 3**, likely due to a different ion bombardment during film growth. With increasing film thickness d, R decreases for films $d < 10$ nm and is constant for films $d > 10$ nm. Using the method of Remeš et al.[4] with H concentration from infrared absorption, the density of our films with $d > 10$ nm is 2.1 g cm^{-3} for the 200 W film, 2.16 g cm^{-3} for the 300 W film, and 2.2 g cm^{-3} for the 400 W film. The density of films with $d < 10$ nm (not given, since the H content determined by FTIR is very uncertain for these films) can be significant lower, which agrees with the increase of R at lower thickness d indicating a void-rich film.[11] This increase of R can be assigned to a

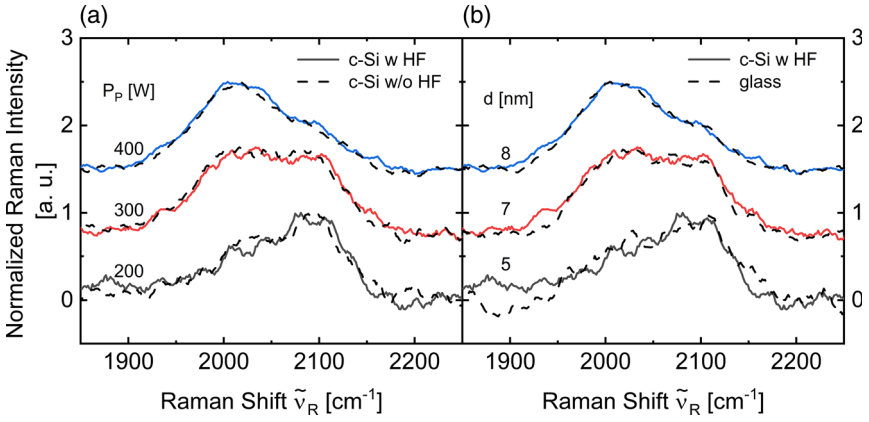

Figure 2. Raman intensity spectra normalized by its maximum of an intrinsic a-Si:H layer on a HF-etched c-Si substrate compared with a) a-Si:H layers from the same deposition on c-Si substrates with a native silicon oxide and b) a-Si:H layers from the same deposition grown on glass. The plasma power was varied from 200 W to 400 W in 100 W steps (indicated on the left in (a) resulting in thicknesses of 5 to 8 nm (indicated on the left in (b)).

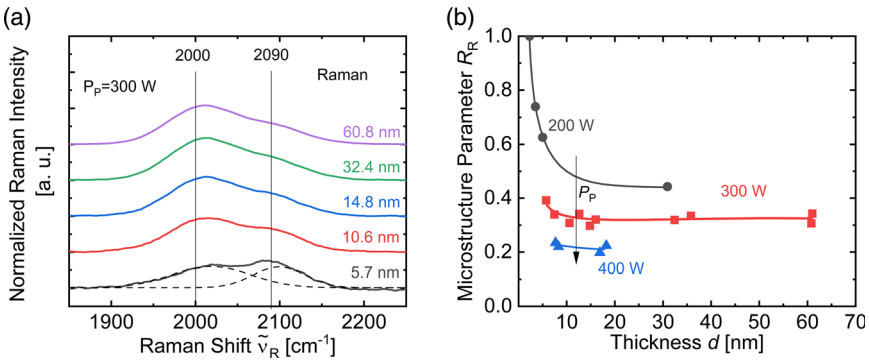

Figure 3. a) Raman spectra of intrinsic a-Si:H layers of various thickness deposited at $P_P = 300$ W versus the Raman shift $\tilde{\nu}_R$. The sample thicknesses are indicated on the right side of the graph. The dashed lines show the double Gaussian function fits for the film of 5.7 nm thickness. b) Layer thickness dependency of R determined from Raman spectroscopy spectra of intrinsic a-Si:H layers with thicknesses of 2.3–60.8 nm and plasma powers of 200, 300, and 400 W. The lines are guides to the eye.

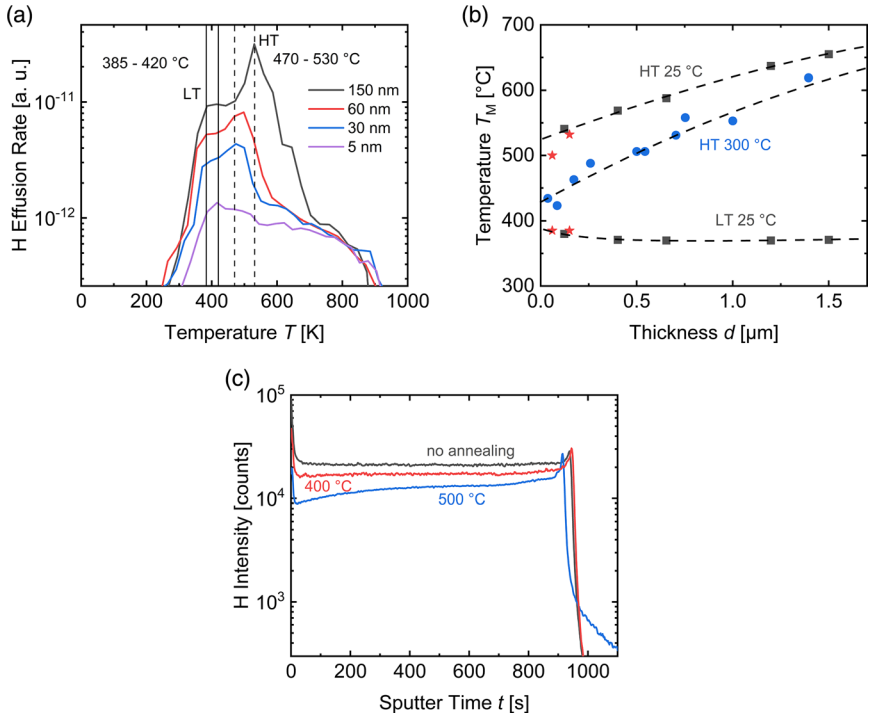

Figure 4. a) Hydrogen effusion rates with a ramping rate of 20 °C min^{-1} for films with a thickness of 5 to 150 nm prepared at $P_P = 300$ W. The straight and dashed lines indicate the minimum and maximum position of the LT peak and HT peak, respectively. b) Temperature T_M of local effusion rate maxima versus the film thickness taken from Beyer and Wagner[13] for high (circle) and low (square) density PECVD films deposited at 300 and 25 °C, respectively. The red stars indicate the high and low temperatures (HT and LT) of maximum effusion of the 60 and 150 nm films from (a). c) SIMS depth profiles of 150 nm films without annealing (black), after annealing at 400 °C (red) and after annealing at 500 °C (blue).

different microstructure of the nucleation layer of the a-Si:H film,[12] showing that the nucleation layer of our underdense material is smaller than 10 nm.

The H effusion rate versus temperature depends on the H diffusion mechanism in a-Si:H[8] and is depicted in **Figure 4**a for films deposited at $P_P = 300$ W with thicknesses of 5 to 150 nm. The 60 and 150 nm films show a low temperature (LT) peak at 385 °C in agreement with diffusion of molecular hydrogen.[8,13] In Figure 4c, a SIMS measurement on the sample with $d = 150$ nm annealed up to 400 °C showed a reduced hydrogen content with a plateau-like diffusion depths profile which also indicate a rapid out diffusion of molecular hydrogen via interconnected voids in ref. [14], pp. 220–222. In contrast after annealing up to 500 °C, the H content follows an error-function-like diffusion profile near the a-Si:H surface (i.e., for sputter times from 0 to 300 s), which indicates additional atomic H diffusion in ref. [14], pp. 222–225. In agreement with the SIMS results, the appearance of a high-temperature (HT) peak in the effusion measurements has been attributed to the formation of dense material by material reconstruction after the loss of H.[8] The shift of the HT peak in Figure 4a to higher T with increasing film thickness agrees with the thickness dependence of the HT-curve of the low (25 °C) deposition temperature a-Si:H (low film density/high hydrogen density) reported by Beyer and Wagner[13] and depicted in Figure 4b. The curve differs considerably from that of dense a-Si:H (300 °C deposition temperature, only HT peak, no LT peak) also shown. These results support that the network in underdense a-Si:H may be similar to the widely investigated low substrate temperature a-Si:H. For the films with a thickness below 60 nm, the LT peak shifts to slightly higher values and the HT peak to lower values, which is also consistent with the trend of the data of Beyer and Wagner.[13] The HT and LT effusion peak positions for these films are not shown in Figure 4b because they are at similar temperatures and difficult to separate.

To investigate the passivation using underdense a-Si:H, we prepared solar cells with varying (underdense) i1-layer thickness on the rear side. For the i1-layer, we used the same recipe as for the above investigated films with a plasma power of 200 W. The deposition time of the i1-layer was set to 2, 3, and 4 s, what should correspond to film thicknesses between 1 and 3 nm. An increase of the i1-layer thickness should increase the R of the a-Si:H i1/i2/p layer stack (total thickness $d = 15$ nm), since the i1-layer is underdense and void rich in contrast to the i2- and p-layer. **Figure 5**f shows the spectra of the three solar cell variations and indeed we see a slight increase of the 2100 cm^{-1} peak with increasing deposition time for the i1-layer since it attributes because of its low thickness to only a small fraction of the measured layer stack to the R. Figure 5a–e shows the JV parameters of the solar cells. V_{OC} and pFF increase with increasing i1-layer thickness. Both parameters increase with improved passivation (higher carrier lifetime).[15] The low value

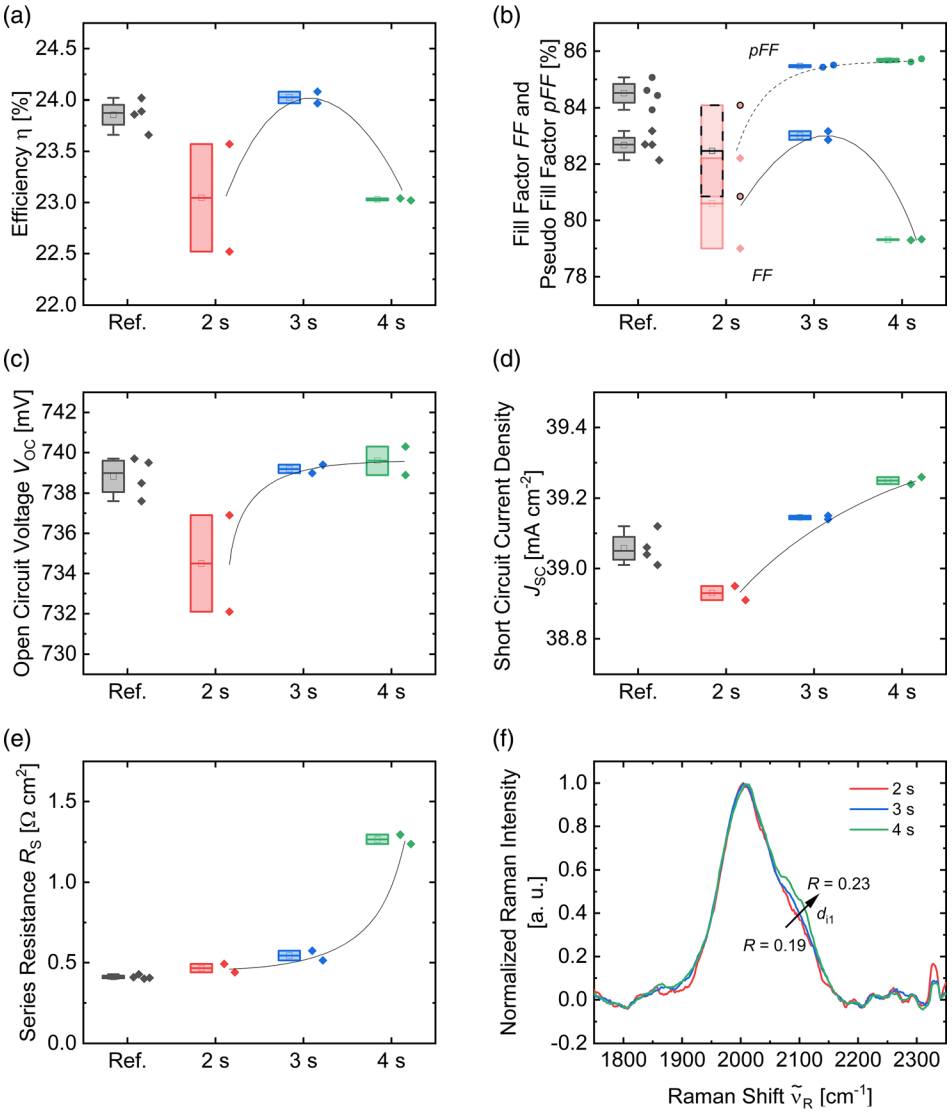

Figure 5. a) Efficiency, b) fill factor and pseudo fill factor, c) open-circuit voltage, d) short-circuit current density, and e) series resistance versus the process time of the rear-side i1-layer deposition. The deposition time of 2, 3, and 4 s should correspond to film thicknesses between 1 and 3 nm. "Ref" represents parameters of baseline solar cells produced as described in Duan et al.[19] f) Raman spectra of the rear side (i1/i2/*p* layer stack) of those solar cells.

and scattering of V_{OC} and pFF for the 2 s deposition might result from a low total amount of molecular hydrogen in the thin layer with $d < 2$ nm and inhomogeneous film coverage because of the island-like growth within the nucleation region.[10,12] The solar cells with 3 and 4 s i1-layer deposition time have similar V_{OC} and pFF which agrees with the hypothesis that the passivation is made by molecular hydrogen from the i1-layer and not by atomic hydrogen from the i2-layer. Otherwise, the passivation would decrease for thicker i1-layers, since it is detrimental for the atomic hydrogen diffusion from the i2-layer to the c-Si.[16,17] The series resistance increases with increasing i1-layer thickness as also found by Luderer et al.[18]. The increase of both R_S and the passivation results in an efficiency maximum for the solar cells with an i1-layer deposited for 3 s ($d_{i1} \approx 2$ nm) and a maximum cell efficiency of 24.1%.

3. Discussion

Underdense a-Si:H is used as i1-layer in the SHJ solar cell fabrication.[1–3,19] This layer is intended to improve the passivation of the c-Si surface by avoiding an epitaxial growth using a fast (>1 nm s^{-1}) and disordered growth instead. The similar Raman spectra of layers grown on different substrate during one deposition process with thicknesses of 5 to 8 nm shown in Figure 2 agree with a lack of epitaxy. For layers including epitaxial growth on the HF-etched c-Si surface, a strongly reduced H content and a microstructure parameter close to 1 would be expected. The microstructure of the (nonepitaxial) layer on the glass substrate would be significantly different. The similar Raman spectra for layers on different substrates therefore indicate a similar growth mechanism for all investigated substrate

materials resulting in a void rich material in particular at low plasma power, presumably due to the rather low self-bias.[20,21] R measured by Raman spectroscopy is thickness independent for layers above 10 nm, while R rises for layer thicknesses <10 nm. This latter increase is likely related to an a-Si:H nucleation layer. The presence of a nucleation layer of about 10 nm or less has also been modeled by, Canillas et al.,[10] Fujiwara et al.,[12] and Li et al.[22]. Furthermore, the solar cell results show that the island-like growth during the nucleation[10,22] already results in a wide area covering film for thicknesses > 2 nm since the passivation quality for i1-layers with $d_{i1} > 2$ nm is constant. The high microstructure parameter (especially for films <5 nm) shown in Figure 3 and the effusion peak near 385 °C as well as the plateau-like H diffusion SIMS profiles for annealing at 400 °C in Figure 4 show that our "underdense" films are highly porous and the H diffusion is dominated by molecular H_2 instead of atomic H. In agreement with this, recently An et al.[23] also stated that the passivation quality highly depends on the low-temperature H effusion characteristics. This indicates that for the good passivation as achieved with underdense a-Si:H,[1,3,19] the c-Si is passivated by dissociative absorption of H_2[24] and not by diffusion of atomic hydrogen to the silicon dangling or reconstructed bonds. This agrees with the fact that the passivation is independent of the i1-layer thickness for $d_{i1} > 2$ nm as shown in Figure 5, since a thicker i1-layer would hinder the atomic H diffusion from the i2-layer. The role of the second, more dense a-Si:H i2-layer, which is needed to achieve high passivation in combination with the i1-layer,[25] may be to keep the H_2 next to the c-Si surface.

4. Conclusion

The "underdense" a-Si:H resembles both in Raman and H effusion the "low-temperature" a-Si:H, whose properties have been discussed extensively in the past. The high H concentration and porosity of this material apparently prevent epitaxy. Varying the thickness of the underdense i1-layer on the rear side of our solar cells, we achieved a maximum efficiency of 24.1%. Our material investigation shows that hydrogen diffusion in underdense a-Si:H is mainly by molecular H_2. Therefore, the successful passivation mechanism of underdense a-Si:H in direct contact with c-Si is probably due to mobile H_2 molecules rather than diffusion of atomic H. We propose that the underdense structure facilitates H_2 diffusion to the interface between c-Si and a-Si:H. The dissociative adsorption of H_2 molecules leads to the silicon passivation at the interface.

5. Experimental Section

For the underdense a-Si:H film preparation, an AK1000 plasma-enhanced chemical vapor deposition (PECVD) system from Meyer Burger using a plasma frequency of 13.56 MHz, an electrode area of (50×50) cm^2, and an electrode substrate distance of approximately 1.7 cm was used. The substrate temperature T, pressure p, and silane flow Q_{SiH4} were set to $T = 200$ °C, $p = 2.7$ mbar, and $Q_{SiH4} = 145$ sccm, respectively. The plasma power P_P was varied from 200 W (80 mW cm^{-2}) to 400 W (160 mW cm^{-2}) in 100 W steps. The layers were prepared on HF-etched polished p-type high resistivity c-Si (100) float-zone wafers (525 µm, 20 Ωcm). In addition, some layers were also prepared on polished wafers with native oxide as well as Corning glass type Eagle 2000. The solar cells were prepared as described by Duan et al.,[19] but for the i1-layer on the rear-(p-)side, we used underdense a-Si:H deposited with $P_P = 200$ W. The J–V curves of the solar cells were measured under standard test conditions (AM1.5, 25 °C, and 100 mW cm^{-2}) by the integrated solar cell analysis system LOANA from pv-tools with a Wavelabs Sinus 220 LED light source. The film thickness was measured using a T-Solar/M2000 spectroscopic ellipsometer from J.A. Woollam. Fourier transform infrared spectroscopy (FTIR) measurements were made by a Nicolet 5700 system from Thermo Electron Corporation, and the Raman spectroscopy measurements were done in back scattering configuration using a Renishaw inVia Raman spectrometer with a 532 nm laser. The microstructure parameter R measured by Raman was calculated similar to the standard procedure for FTIR measurements by $R = I_{2100}/(I_{2100} + I_{2000})$.[26,27] The peak intensities I_{2000} and I_{2100} are defined as the areas below two Gaussian functions fitted to the Raman intensity with peak centers near the wavenumbers of 2000 and 2100 cm^{-1}, respectively.[28] Hydrogen effusion was measured as described elsewhere[29] using a heating rate of 20 °C min^{-1}. The secondary ion mass spectrometry (SIMS) was made by a time-to-flight setup with a cesium sputtering beam and a sputtering energy of 1 keV on an area of (300×300) µm^2.

Acknowledgements

The authors gratefully acknowledge Dr. Wolfhard Beyer who has made a great contribution to this work but passed away too early. His pioneering work in the field has been a source of inspiration for many, and his contributions have left a lasting impact on the scientific community. We are grateful for the guidance and mentorship he provided.

Open Access funding enabled and organized by Projekt DEAL.

Conflict of Interest

The authors declare no conflict of interest.

Data Availability Statement

The data that support the findings of this study are available from the corresponding author upon reasonable request.

Keywords

amorphous silicon, passivation, silicon heterojunctions, solar cells, underdense materials

Received: February 10, 2023
Revised: March 6, 2023
Published online: March 18, 2023

[1] W. Liu, L. Zhang, R. Chen, F. Meng, W. Guo, J. Bao, Z. Liu, *J. Appl. Phys.* **2016**, *120*, 175301.
[2] H. Sai, P.-W. Chen, H.-J. Hsu, T. Matsui, S. Nunomura, K. Matsubara, *J. Appl. Phys.* **2018**, *124*, 103102.
[3] X. Ru, M. Qu, J. Wang, T. Ruan, M. Yang, F. Peng, W. Long, K. Zheng, H. Yan, X. Xu, *Sol. Energy Mater. Sol. Cells* **2020**, *215*, 110643.
[4] Z. Remeš, M. Vaněček, P. Torres, U. Kroll, A. H. Mahan, R. S. Crandall, *J. Non-Cryst. Solids* **1998**, *227–230*, 876.
[5] J. S. Custer, M. O. Thompson, D. C. Jacobson, J. M. Poate, S. Roorda, W. C. Sinke, F. Spaepen, *Appl. Phys. Lett.* **1994**, *64*, 437.
[6] D. L. Williamson, *MRS Proc.* **1995**, *377*, 251.
[7] H. Fritzsche, M. Tanielian, C. C. Tsai, P. J. Gaczi, *J. Appl. Phys.* **1979**, *50*, 3366.
[8] W. Beyer, H. Wagner, *J. Non-Cryst. Solids* **1983**, *59–60*, 161.

[9] Y. Huang, Y. Zeng, Z. Zhang, X. Guo, M. Liao, C. Shou, S. Huang, B. Yan, J. Ye, *Sol. Energy Mater. Sol. Cells* **2019**, *192*, 154.
[10] A. Canillas, E. Bertran, J. L. Andújar, B. Drévillon, *J. Appl. Phys.* **1990**, *68*, 2752.
[11] H. Wagner, W. Beyer, *Solid State Commun.* **1983**, *48*, 585.
[12] H. Fujiwara, Y. Toyoshima, M. Kondo, A. Matsuda, *Phys. Rev. B* **1999**, *60*, 13598.
[13] W. Beyer, H. Wagner, *J. Phys. Colloques* **1981**, *42*, C4-783.
[14] W. Beyer, *Semiconductors and Semimetals* (Ed: N. H. Nickel), vol. *61*, Academic Press, San Diego **1999**, pp. 165–239, https://doi.org/10.1016/S0080-8784(08)62707-6.
[15] M. R. Page, E. Iwaniczko, Y. Xu, L. Roybal, R. E. Bauer, H.-C. Yuan, Q. Wang, D. L. Meier, in *2008 33rd IEEE Photovoltaic Specialists Conf.*, IEEE, San Diego May **2008**, pp. 1–4, https://doi.org/10.1109/PVSC.2008.4922683.
[16] D. E. Carlson, C. W. Magee, *Appl. Phys. Lett.* **1978**, *33*, 81.
[17] W. Beyer, H. Wagner, *J. Appl. Phys.* **1982**, *53*, 8745.
[18] C. Luderer, D. Kurt, A. Moldovan, M. Hermle, M. Bivour, *Sol. Energy Mater. Sol. Cells* **2022**, *238*, 111412.
[19] W. Duan, A. Lambertz, K. Bittkau, D. Qiu, K. Qiu, U. Rau, K. Ding, *Prog. Photovoltaics Res. Appl.* **2022**, *30*, 384.
[20] Y. Kuo, *J. Electrochem. Soc.* **1990**, *137*, 1235.
[21] N. Maître, T. Girardeau, S. Camelio, A. Barranco, D. Vouagner, E. Breelle, *Diamond Relat. Mater.* **2003**, *12*, 988.
[22] D. Li, G. L. Liu, Y. Yang, J. H. Wu, Z. R. Huang, *J. Nanomater.* **2013**, *1–7*, 2013.
[23] J.-H. An, J.-H. Oh, K. T. Jeong, O. Kwon, S. J. Oh, K.-H. Kim, S.-W. Kim, M. J. Keum, H. Song, K.-H. Kim, *ACS Appl. Energy Mater.* **2022**, *5*, 15029.
[24] M. Dürr, U. Höfer, *Surf. Sci. Rep.* **2006**, *61*, 465.
[25] H. Sai, H.-J. Hsu, P.-W. Chen, P.-L. Chen, T. Matsui, *Phys. Status Solidi A* **2021**, *218*, 2000743.
[26] D. Jousse, E. Bustarret, F. Boulitrop, *Solid State Commun.* **1985**, *55*, 435.
[27] A. H. Mahan, P. Raboisson, R. Tsu, *Appl. Phys. Lett.* **1987**, *50*, 335.
[28] C. Maurer, S. Haas, W. Beyer, F. C. Maier, U. Zastrow, M. Hülsbeck, U. Breuer, U. Rau, *Thin Solid Films* **2018**, *653*, 223.
[29] W. Beyer, F. Einsele, *Advanced Characterization Techniques for Thin Film Solar Cells* (Eds: D. Abou-Ras, T. Kirchartz, U. Rau), Wiley-VCH Verlag GmbH & Co. KGaA, Weinheim **2016**, pp. 569–595, https://doi.org/10.1002/9783527699025.ch20.